Deposition law of flat fan nozzle for pesticide application in horticultural plants

Xiaoyi Wu[1], Yalan Jia[2], Bo Luo[2], Chongchong Chen[1], Yaxiong Wang[1*], Feng Kang[1], Jiale Li[1]

(1. *School of Technology, Beijing Forestry University, Key Lab of State Forestry Administration for Forestry Equipment and Automation, Beijing100083, China*; 2. *Army Aviation Institute, Beijing 101123, China*)

Abstract: Pesticide spraying is to protect the plants with adequate target coverage and a minimum of off-target drift. Understanding the spatial distribution characteristics of spray droplets is essential for regulating pesticide deposition, in order to investigate the relationship between the two at the mechanistic level and provide an accurate basis for nozzle selection, this study compared the characteristics of the atomization field under different pressures, angles, and flow rate types by phase Doppler particle analyzer (PDPA), the unit spatial density of droplet was used as a link to explore the internal mechanism that affects the deposition efficiency by constructing a transport model and conducting actual spraying experiments. The results showed that the cumulative distribution of droplet diameter could be perfectly fitted by the Rosin-Rammler correlation, and the deposition efficiency had a strong correlation with the peak particle size range. For strawberry and chrysanthemum plants, the optimal droplet deposition particle size ranges were 250-270 μm and 240-260 μm, respectively. This article explained the deposition efficiency from a single droplet dynamics mechanism and deposition of droplet cloud, which provided a new research idea for the study of precision plant protection.

Keywords: pesticide transport, deposition, atomization field, PDPA

DOI: 10.25165/j.ijabe.20221504.7502

Citation: Wu X Y, Jia Y L, Luo B, Chen C C, Wang Y X, Kang F, et al. Deposition law of flat fan nozzle for pesticide application in horticultural plants. Int J Agric & Biol Eng, 2022; 15(4): 27–38.

1 Introduction

Pesticide is an important global agricultural production material that provides a strong guarantee for the realization of agricultural production and bumper harvests. Improving the utilization and understanding of the behavior of agrichemical sprays applied to plants has been a long-standing challenge[1-3]. The research aims to promote the high retention rate of pesticides in plant targets, the droplet deposition is more complicated because of many influence factors, such as canopy structure and row spacing, which may cause variability quiet in the spray retention efficiency of plants[4, 5]. High retention on plants is important, as spray drift is one of the main pollution sources identified when pesticides (also known as plant protection products, PPP) are applied to plants[6]. Harmful effects of pesticides on humans and the environment are known for years[7]. There are approximately 25 million pesticide poisoning incidents in the world every year[8]. The potential adverse consequences of PPP usage can be significantly dispersed along with time and space[9]. Exploring the deposition characteristics of nozzles and reducing spray drift are the core tasks in current scientific research.

At present, a single droplet and the droplet cloud have been investigated as separate subjects. The former focuses on the dynamics of a single droplet impacting the surface in order to discern the impact behavior. When a single droplet hits the solid surface, the kinetic energy changes from the normal direction to the tangential direction and the droplet rapidly diffuses outward. When the inertial force of the impact is greater than the capillary force holding the droplet together, the droplet breaks up, otherwise, it will continue to spread until kinetic energy is exhausted. In the process of diffusion, part of the kinetic energy is dissipated in viscosity and the other part is converted into surface energy. At this point, the geometrical shape of the droplet is usually a flat disk with a thick edge of a free circle layer around it. The diameter when the droplet diffuses to the maximum extent is called the maximum diffusion diameter. If the surface energy of the droplet is still high, the droplet will undergo a recoil stage, which will lead to splashing or rebounding[10,11]. Researchers have studied the influence of the particle size, velocity, deposition surface characteristics, and other factors on the droplet hitting the wall behavior[12-15], so as to derive the behavior judgment equations[16-19]. A bounce criterion was first presented by Mao et al.[18], who predicted bounce via a series of energy balance arguments which considered the spread and recoil stages of impact. However, Mao et al.[18] only considered droplets impacting a horizontal surface from directly above. Dorr et al.[16] extended this work to consider impact at any angle of impingement, and any inclination of the leaf surface, which also calculated "excess rebound energy" (E_{ERE}) to predict the occurrence of rebound. E_{ERE} was selected for the droplet rebound part of the model in this article. The occurrence of splash is related to the capillary effect. In order to determine

Received date: 2021-11-15 **Accepted date:** 2022-03-31

Biographies: **Xiaoyi Wu**, Master candidate, research interest: precision plant protection, Email: wuxiaoyi@bjfu.edu.cn; **Yalan Jia**, Master, research interest: precision plant protection, Email: jiayalany@163.com; **Bo Luo**, Master, research interest: precision plant protection, Email: hblobo@163.com; **Chongchong Chen**, Master candidate, research interest: precision plant protection, Email: chenchongchong@bjfu.edu.cn; **Feng Kang**, PhD, Professor, research interest: forestry engineering. Email: kangfeng98@bjfu.edu.cn; **Jiale Li**, Master candidate, research interest: precision plant protection, Email: lijiale@bjfu.edu.cn.

***Corresponding authors**: **Yaxiong Wang**, PhD, Graduate teacher, research interest: precision plant protection. School of Technology, Beijing Forestry University, Beijing 100083, China. Tel: +86-10-62336137-709, Email: yaxiongwang87@bjfu.edu.cn.

whether splashing can occur, Mundo et al.[19] and Forster et al.[17] proposed a splash threshold determination equation. The relevant parameters include the droplet's properties, velocity, and surface characteristics. When the calculated value related to the droplet properties is greater than the corresponding threshold related to the deposition surface, it is determined that the splash occurs.

The interaction among the droplets as well as the actual atomization field shape and canopy structure are considered in the droplet cloud study. These can be divided into two types: those are to capture the movement information of the droplets in the atomization field, describe the characteristics of the atomization field[20-22], and find the relationship between them and the deposition[23]. Nozzle types are usually defined into six spray categories based on rough classification, viz.: Extremely fine (XF), Very Fine (VF), Fine (F), Medium (M), Coarse (C), Very Coarse (VC), and Extremely Coarse (XC), Ultra coarse (UC)[24]. Methods for accurately describing the nozzle atomization field have also been developed, including Phase Doppler particle analysis (PDPA)[25], laser diffraction analysis[26], particle measuring system (PMS)[27], and particle droplet imaging analysis[28]. Torrent et al.[29] tested several common models by three indirect methods: PDPA and two different wind tunnels, the main purpose of which was to classify hollow-cone nozzle models. Zhang et al.[30] used a laser diffraction technique in wind tunnel to provide information on droplet size distribution and spectra. However, this method ignores the impact of collision behavior on deposition. The other kind of research calculates deposition through actual experiments or simulations[31-33], including direct measurement[34-36] of target deposition and indirect measurement[37-41] reflected by the amount of drift in the air and on the ground[42-44]. Spraying experiments usually only consider the relationship between initial variables and deposition efficiency. Bolat et al.[45] conducted spray performance tests with three different nozzle types and four velocity conditions as initial variables. Deren et al.[46] compared the zinc deposits on soybean plants at three developmental stages under different nozzle types and spray pressures. Experimental fitting plays an important role but weakens the theoretical basis. In addition, Numerical simulation technology has gradually increased in deposition research applications in recent years, but the parameter settings are highly dependent on experimental data.

In general, the theory of a single droplet impact surface should be incorporated into droplet cloud studies in a suitable way to improve understanding of deposition mechanisms and to make nozzle selection recommendations more relevant. In this work, PDPA was used to determine the atomization field characteristics produced by the nozzle under different pressures, flow rate types, and spray angles. Strawberry plants and chrysanthemum plants were selected as objects, the behaviors (adhere, bounce, and shatter) of droplets in the experimental area were distinguished by the single droplet impact theory, and the deposition efficiency per unit leaf area was calculated by indoor spraying experiment. According to the initial distribution characteristics of droplets in the atomization field and the calculation results of the model, the discovery of regularity between nozzle atomization field characteristics and deposition efficiency was explored.

2 Material and methods

2.1 Droplet characterization using a PDPA

Figure 1 shows the spray experimental system. The droplet size spectrum was characterized using a Phase Doppler Particle Analyzer device (TSI, Inc., Minnesota, USA). According to the laser debugging position, the system parameter settings are listed in Table 1. A 3DOF mobile platform was used to control the measurement position precisely. A total of eight spray combinations were measured in the PDPA experiment, and the combinations are listed in Table 2. The equivalent outlet diameter is the nozzle outlet diameter corresponding to different flow types. Flat fan nozzles (Teejet, Illinois, USA) were chosen for the experiments, which are the most commonly used in spraying.

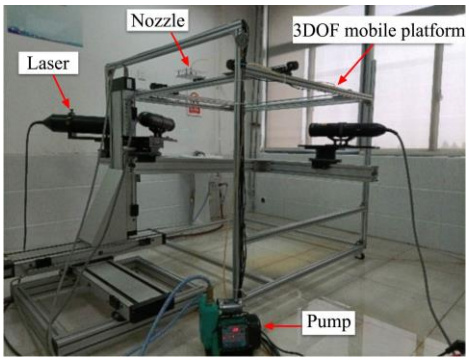

Figure 1 PDPA test system

Table 1 PDPA system parameter settings

Item	Channel 1	Channel 2	Channel 3
PMT voltage/V	630.0	400.0	630.0
Burst threshold/mV	55.0	45.0	55.0
Downmix frequency/MHz	38.5	38.5	38.5

Table 2 All spray combinations in the PDPA experiment

Nozzle	Spray angle/(°)	Pressure/MPa	Equivalent outlet diameter/mm
FF6502	65	0.25	0.8
FF6504	65	0.15	1.2
FF6504	65	0.25	1.2
FF6504	65	0.35	1.2
FF6506	65	0.25	1.5
FF8004	80	0.25	1.2
FF11004	110	0.25	1.2
FF11006	110	0.25	1.5

In all tests, the nozzle position was 0.5 m above the measuring point for all flat-fan nozzles in order to simulate the actual spraying. To sample the whole willow cross section, the scanning trajectory takes the form of an “S” shaped route measurement with an interval of 0.01 m or 0.02 m along the *X*-axis and 0.01 m along the *Y*-axis. Figure 2 shows the measurement route of the data points in the experiment. Three repeats were conducted at each measurement point, and at least 5000 droplets were measured per repeat to ensure the data accuracy of the measurement. The average value of the three measurements was thereby taken as the droplet velocity and size at the measurement point.

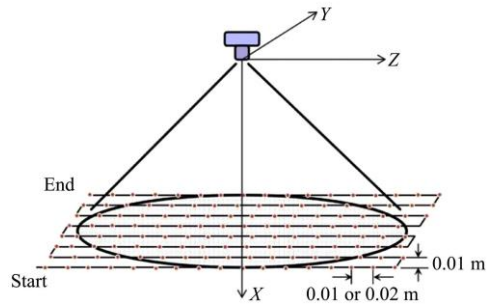

Figure 2 Scanning path during PDPA droplet size characterization

Tap water was used as spray liquid for all nozzles. All measurements were performed in an air-conditioned room at (20±1)℃ at 55%-65% of relative humidity. Three repeats for each nozzle model were carried out. Each repeat was performed with a different single nozzle unit, so three different units were tested for each model. Measurement acquisition was performed with the software FlowSizer 64 (TSI, Inc., Minnesota, USA).

2.2 Model description

2.2.1 Droplet statistical model

Relative span (*RS*) is used to describe the uniformity of the initial particle size distribution of the nozzle[47], defined as,

$$RS=(D_{v90}-D_{v10})/D_{v50} \tag{1}$$

The Rosin-Rammler function is a widely used distribution function to characterize the initial particle size of spray droplets, as shown in Equation (2).

$$y=1-\exp(-(D/D_0)^{\delta}) \tag{2}$$

where, D is the diameter of spray droplet, mm; y is the cumulative fraction of droplets less than the particle size D, %; δ is the "uniformity constant"; D_0 is the characteristic particle size, which means that the cumulative mass of droplets smaller than this size accounts for 63.2%, mm.

2.2.2 Droplet transport models

The key parameters describing impaction are the droplet diameter D (mm), the droplet impact velocity v (m/s), the fluid density ρ (kg/m^3), the fluid viscosity μ (kg/m·s), the fluid-air surface tension σ (kg/s^2), the static contact angle θ_e (°), and the impingement angle α (°). The impingement angle is defined as the angle between the impact trajectory and the leaf surface tangent plane at the site of impaction.

A droplet is predicted to shatter on impact if[17,19]:

$$K = Oh(Re_n)^{1.25} = We_n^{0.5}Re_n^{0.25} > K_{crit} \tag{3}$$

K describes the fluid and droplet properties, and K_{crit} is a critical value related to the properties of the surface being impacted.

The Ohnesorge (Oh) number is

$$Oh = \mu / \sqrt{\rho D\sigma} \tag{4}$$

The Weber (We) number is

$$We = \rho D V_n^2 / \sigma \tag{5}$$

The Reynolds (Re) number is

$$Re = \rho D V_n / \mu \tag{6}$$

where, the velocity is calculated as the component of velocity normal to the impacted surface by the follows:

$$v_n = v\sin\alpha \tag{7}$$

The value of K_{crit} can be calculated according to the following equations[17].

$$K_{crit} = -0.584(CA_{20\%acetone})+147 \tag{8}$$

$$K_{crit} = -0.9227(CA_{50\%acetone})+160 \tag{9}$$

where, $CA_{20\%acetone}$ and $CA_{50\%acetone}$ are the static contact angles made by a droplet of either 20% acetone or 50% acetone on the leaf surface. Acetone measurements are relative standard values and do not change when used. In this experiment, the macro video lenses Zoom7000 (Navitar, New York, USA) was used to measure the contact angle, and we took the average of these two equations as our value for K_{crit} [35].

In addition, the droplets will adhere or rebound if $K \le K_{crit}$. The accurate behavior can be further judged in combination with the excess rebound energy. This article adopts the rebound equation improved by Dorr et al.[35]. The "excess rebound energy" (E_{ERE}) remaining energy equation is expressed as:

$$E_{ERE} = \left[\frac{\pi}{4}D_{major}^2(1-\cos\theta_e)+\frac{2}{3}\pi\frac{D^3}{D_{major}}\right]\sigma - 0.12\pi D^2\sigma\left(\frac{D_{major}}{D}\right)^{2.3}(1-\cos\theta_e)^{0.63} - \pi\sigma D^2 \tag{10}$$

where, D_{major} is an equivalent diameter, which can be solved by the following equations:

$$D_{major} = \frac{D_{normal}^2}{D_{minor}} \tag{11}$$

$$\left[\frac{1}{4}(1-\cos\theta_e)+0.2\frac{We^{0.83}}{Re^{0.33}}\right]\left(\frac{D_{normal}}{D}\right)^3-\left(\frac{We}{12}+1\right)\left(\frac{D_{normal}}{D}\right)+\frac{2}{3}=0 \tag{12}$$

$$\left[\frac{1}{4}(1-\cos\theta_e)+0.2\frac{We_n^{0.83}}{Re_n^{0.33}}\right]\left(\frac{D_{minor}}{D}\right)^3-\left(\frac{We_n}{12}+1\right)\left(\frac{D_{minor}}{D}\right)+\frac{2}{3}=0 \tag{13}$$

If a real solution to (10) does not exist, or D_{normal} is calculated to be less than D, set $D_{normal} = D$ as a minimum bound. The notation We_n and Re_n denote the Weber and Reynolds numbers computed with v_n rather than v. If $D_{minor} < D$, then we set D_{minor} as a correction. If the criterion is met:

$$E_{ERE} > 0 \tag{14}$$

Then, there is sufficient energy for bounce to occur.

In this study, shatter takes precedence over bounce. That is, it is assumed that bounce may only occur if shatter does not take place during the spreading process. Therefore, if both bounce and shatter criteria (Equations (3) and (14)) are met, shatter is the predicted outcome. Table 3 helps to understand more accurately. The PDPA measurement results are sorted corresponding to particle size and velocity. For each nozzle, the area of the actual spraying area is selected for the calculation of behavior judgment.

Table 3 Judgment of droplet behavior based on theoretical equation

Excess rebound energy	Shatter threshold	
	$K > K_{crit}$	$K < K_{crit}$
$E > 0$	Shatter	Bounce
$E < 0$	Shatter	Adhere

Note: E-Excess rebound energy; K-The fluid and droplet properties; K_{crit}-A critical value related to the properties of the surface being impacted

The characteristics of the atomization field are described by PDPA, including droplet size, vertical component velocity, and horizontal component velocity, as well as statistical time and particle number. Taking the time factor into consideration, the spatial density of different droplets was statistically analyzed. The flow rate of droplets per unit time in the measurement area was calculated by Equation (15).

$$V = \frac{4}{3}\pi(N - N_b - N_s)\times 10^{-18}\times\left(\frac{D_{32}}{2}\right)^3 \tag{15}$$

where, V is the volume of the droplet passing through the measurement area per unit time, m^3; D_{32} is the SMD at the selected location, mm; N is the number of particles passing per unit time in the area; N_b is the number of droplets that rebound after calculation by the above model in the same area; N_s is the number of splashed droplets.

The flow rate per unit area in the equation is calculated based on PDPA, and the selected area is the intersection of the three laser beams. The SMD is taken as the average particle diameter of the region. The inter-area flow is calculated using integrals. In

addition, the calculation area is selected by the initial distribution position of the droplets in the atomization field.

2.3 Determination of retention

Figure 3 shows the spraying experimental device. Spray retention was evaluated by a fluorometric method using tartrazine as a chemical tracer at a targeted concentration of 1.0 g/L. Strawberry and chrysanthemum plants were selected as spraying targets. Repeated spraying of fungicides is a common phenomenon in greenhouse cultivation[48]. The nozzle sprays along the guide rail at a constant speed of 1.1 m/s. Nine nozzles were selected and each nozzle was tested at three pressures, which contain all the experimental group categories from the PDPA experiment. These were positioned 0.5 m above the mean plant height, which is the common spray height used in applications[35]. The experiment provided a range of spray droplet spectra, under different pressures, to 10 plants per treatment (5 strawberry plants sprayed at a time with 5 chrysanthemum plants placed on either side of the nozzle, in a line along the direction of the nozzle movement). Artificial targets (×4 LILY 3PCD white round 25 mL, 20 mm diameter, plastic containers), placed similarly under the nozzles, were sprayed in all treatments to accurately confirm the spray volume delivered. The horizontal distance between the target and the moving position of the nozzle was selected by the initial distribution of droplets in the atomization field.

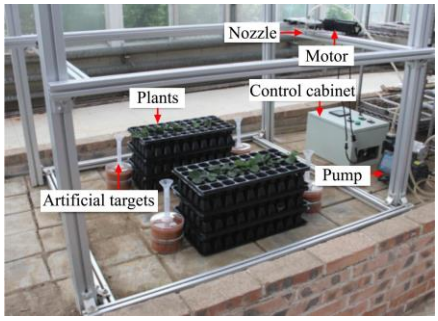

Figure 3 Spraying experimental device

After spraying, the plants were harvested at soil level and total retention for the entire plant was used for the results in the current study. All of the plant material in each repeat was placed into individual beaker and washed in a known volume of deionized water. The artificial targets were also washed in a known volume of deionized water. The tartrazine dye recovered in washes (from plant or artificial target) was quantified by a spectrometer (Daojin, Guangzhou, China) to determine total dye recovery from plant or artificial surfaces at 427 nm. Plant surface areas were determined using Image-J software (National Institutes of Health, Maryland, USA). Percentage plant retention was calculated from the amount of dye recovered per plant unit area divided by the known amount applied per unit area (from artificial surface determinations). Equation (16) is the deposition efficiency equation:

$$A = \frac{m_l / S_l}{m_a / S_a} \times 100\% \tag{16}$$

where, A is the deposition percentage, %; m_l is the leaf surface deposition mass, g; S_l is the leaf area, cm^2; m_a is the target collection mass, g; S_a is the artificial target area, cm^2.

2.4 Statistical analysis

For the case in which an analysis was made of the PDPA methodologies, the results shown in the tables and figures correspond to the mean value of the three sets of parallel experiments made in each case. Treatments were compared using analysis of variance and least significant difference tests (LSD) at P=0.05 to determine the significance of treatments on spray deposits retained by the plant.

3 Results and discussion

3.1 Droplet diameter and velocity

The actual spraying process is mainly sprayed by nozzle groups, which leads to the overlapping phenomenon of droplets at the edge of the atomization field, and there are more small-volume droplets, which are prone to drift and have less effective adhesion to the target. This is why we have adjusted the statistical position of each set of nozzle data so that the edge coincident droplets are not included in the calculation, which can also make the results as close to the actual situation as possible. Table 4 lists the droplet size characteristics of flat fan nozzles with different spray angles and flow rate types (FF6502, FF6504, FF6506, FF8004, FF11004, FF11006), three spray pressures (0.15 MPa, 0.25 MPa, 0.35 MPa) were provided in the experiment.

Table 4 Droplet size spectrum characteristics of the tested nozzles

Type	Pressure/MPa	D_{10}/μm	D_{20} /μm	D_{30}/μm	D_{32}/μm	D_{V10}/μm	D_{V50}/μm	D_{V90}/μm
6502	0.25	245.4	239.1	242.4	249.1	205.0	252.0	323.5
6504	0.15	308.1	311.1	314.2	320.6	268.0	317.5	412.0
6504	0.25	289.5	292.3	295.3	301.3	255.5	297.5	386.0
6504	0.35	284.6	287.6	291.3	298.9	251.0	293.0	385.0
6506	0.25	279.2	283.0	287.7	297.2	244.0	286.0	406.5
8004	0.25	259.9	261.9	263.9	268.0	227.0	276.0	316.5
11004	0.25	248.8	255.2	262.4	277.3	210.0	280.5	396.0
11006	0.25	244.9	246.9	247.8	250.5	224.0	245.0	308.0

3.1.1 Droplet diameter distribution characteristics at different spray pressures

Figures 4a and 4b respectively show the relative mass distributions and cumulative distributions of the droplet diameter of the FF6504 nozzle under three pressures.

Narrowing the initial relative span of the spray could effectively reduce droplet drift. As the spray pressure increased, the *RS* value first decreased and then rose, and the peak point presented the same trend. The cumulative distribution of droplets conformed to the Rosin-Rammler distribution. Table 5 lists the values of D_0, δ, and *RS* under three groups of different pressures. In this paper, *RS* was selected as the indicator of the initial particle size distribution due to the deviation between the fitted curve and the original particle size distribution. As the pressure increased, the value of *D* gradually decreased, which indicated that the degree of liquid film breakage gradually deepened, and the droplet atomization effect became dense.

Table 5 D_0 and δ values of the Rosin-Rammler distribution and *RS* value at different pressures

Type	Pressure/MPa	D_0/μm	δ	*RS*
FF6504	0.15	335.55	7.18	0.45
FF6504	0.25	322.40	6.03	0.43
FF6504	0.35	319.22	4.85	0.46

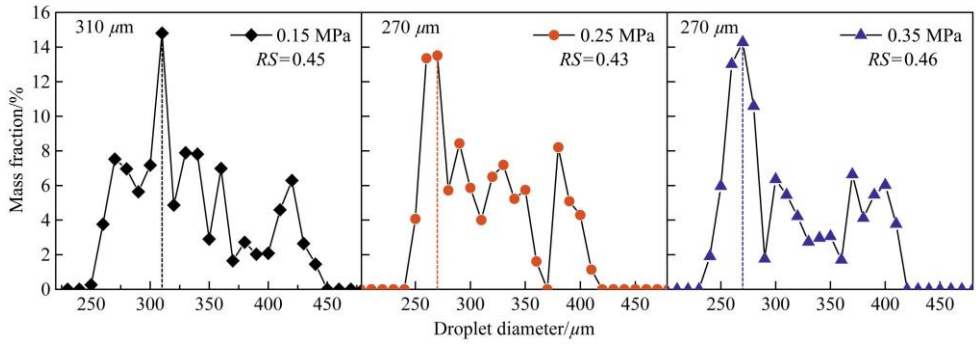

a. Relative mass distributions of droplets diameter

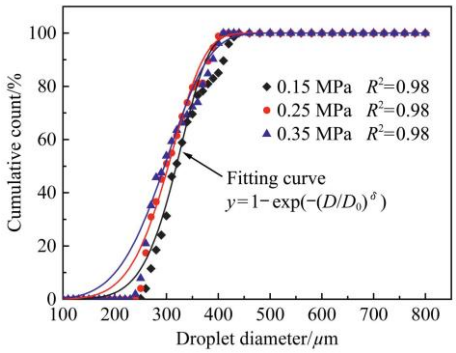

b. Relative cumulative distributions of droplets diameter

Figure 4 Relative mass fraction and cumulative distributions of droplets diameter at three pressures (FF6504)

3.1.2 Droplet diameter distribution characteristics at different flow rate types

Figure 5a shows the relative mass distribution of three nozzles with different flow rate types at a pressure of 0.25 MPa. The peak particle size of FF6504 was 270 μm, which was higher than 240 μm of FF6502 and 250 μm of FF6506. The size of the peak particle size was closely related to the nozzle structure and pressure. Figure 5b is the cumulative distribution of droplet mass of nozzles FF6502, FF6504, and FF6506, which all followed the R-R distribution rule. In Figure 5b, it could be judged that when the flow model of the selected nozzle was too small, the cumulative curve would move to the left under the same pressure and angle. When the initial distribution of the droplets gradually stabilized but the flow rate type continued to increase, the size distribution of the droplets would be more dispersed. The values of D_0, δ, and RS are listed in Table 6.

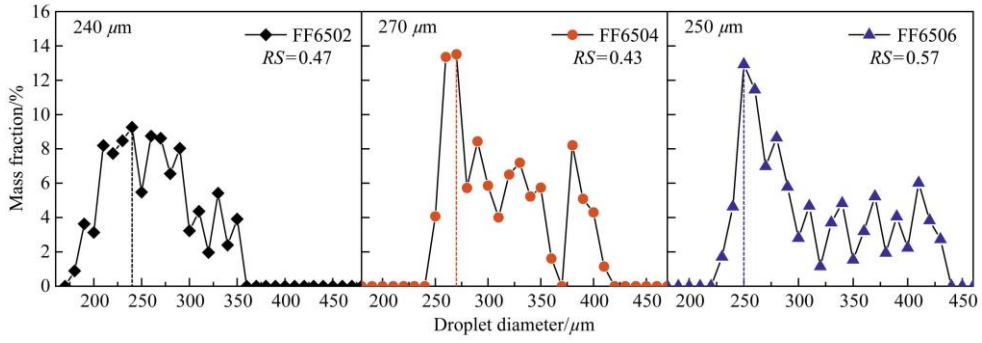

a. Relative mass distributions of droplets diameter

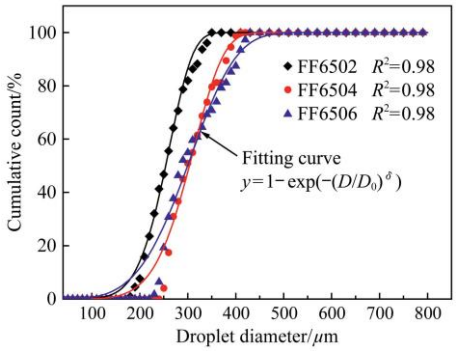

b. Relative cumulative distributions of droplets diameter

Figure 5 Relative mass fraction and cumulative distributions of droplets diameter at three flow types

Table 6 D_0 and δ values of the Rosin-Rammler distribution and RS value at different flow rate types

Type	Pressure/MP	D_0/μm	δ	*RS*
FF6502	0.25	268.90	6.36	0.47
FF6504	0.25	322.40	6.03	0.43
FF6506	0.25	326.64	4.26	0.57

3.1.3 Droplet diameter distribution characteristics at different spray angles

Figures 6a and 6b show the relative mass and cumulative distributions of droplet diameter at different spray angles of 65 °, 80 °, and 110 ° respectively. The peak particle diameters of 65 °, 80 °, and 110 ° in Figure 6a were 270 μm, 310 μm, and 220 μm, respectively. The *RS* value of the FF8004 nozzle was 0.32, indicating that the particle size concentration was the highest and the uniformity was gainful. The *RS* of FF11004 under the same pressure was 0.66, which proved that the spray uniformity was poor. The final spraying effect needs to be further judged in combination with plants. All the distributions were close to Rosin-Rammler distribution patterns. Among them, the nozzle FF8004 curve was at the far left and the characteristic particle size was the smallest, indicating that the cumulative amount reached 100% first. Table 7 lists the D_0, δ, and *RS* of the corresponding nozzle.

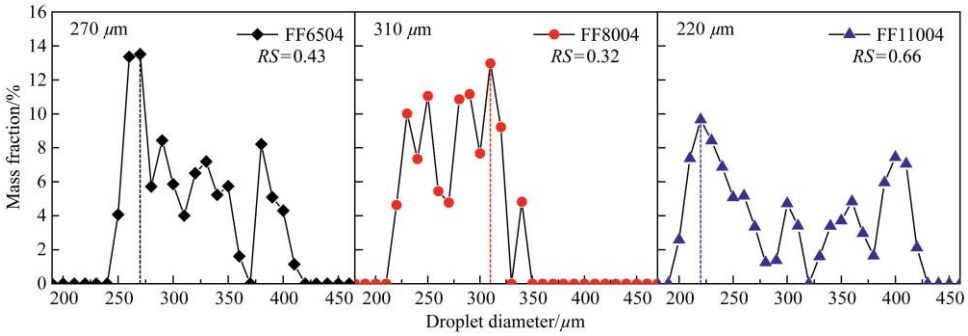

a. Relative mass distributions of droplets diameter

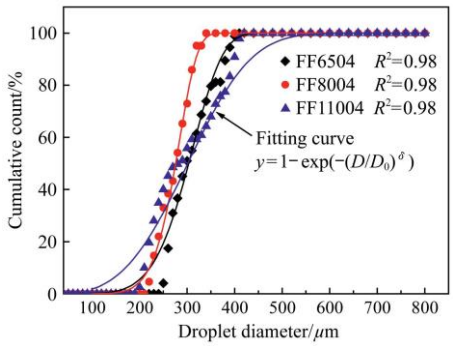

b. Relative cumulative distributions of droplets diameter

Figure 6 Relative mass fraction and cumulative distributions of droplets diameter at three spray angles

Table 7 D_0 and δ values of the Rosin-Rammler distribution and *RS* value at different spray angles

Type	Pressure/MPa	D_0/μm	δ	*RS*
FF6504	0.25	322.40	6.03	0.43
FF8004	0.25	288.12	8.44	0.32
FF11004	0.25	336.88	3.30	0.66

3.1.4 Velocity distribution characteristics of droplets under different spray conditions

Figure 7a presents the relative number distributions of droplet velocity at different pressures of 0.15 MPa, 0.25 MPa, and 0.35 MPa, respectively. The droplet velocity was combined by the horizontal and vertical components. Peak velocity showed an upward trend with increasing pressure in Figure 7a. Figure 7b shows the velocity number distribution of nozzles with different flow rate types under the pressure of 0.25 MPa. The test results showed that the peak velocity of the FF6504 nozzle was the smallest, only 3.26 m/s, but it accounted for the largest proportion of the peak velocity among the three types of nozzles; the FF6506 nozzle had the highest peak velocity, reaching 5.23 m/s, which also had the widest velocity span. Compared with the FF6502 nozzle, the velocity distribution of the FF6504 nozzle moved to the left as a whole, and the changing trend was similar. The velocity distribution of the FF6506 nozzle moved to the right as a whole, which indicates that the increase in the flow rate type would not make the velocity increase or decrease, which might be related to the droplet diameter distribution. The relationship between droplet diameter and velocity distribution was discussed in Section 3.2. Figure 7c shows the velocity distribution of different spray angles at 65 °, 80 °, and 110 ° under the pressure of 0.25 MPa. The peak velocities of nozzles FF8004, FF6504, and FF11004 decreased successively, and the proportion of the peak value also gradually decreased. A higher peak velocity ratio indicated a more concentrated and uniform velocity distribution in the atomization field, which in turn increased the likelihood of similar droplet behavior and made it easier to improve deposition efficiency by adjusting other droplet parameters.

3.2 Correlation between droplet velocity and diameter

Figure 8a shows the variation of SMD and average velocity along with the radial distance from the spray center to the outside (left side) under three pressures, namely, 0.15MPa, 0.25 MPa, and 0.35 MPa. The experimental nozzle was FF6504. D_{32} became larger under the three pressures but the growth rate was different with the increase of the radial distance. The overall trend of the average velocity was similar to D_{32}, the droplet falling velocity in the center of the spray was lower, and the edge velocity was higher. It is easier to understand that high-velocity droplets could travel

farther. The velocity change range from center to edge was the most obvious under the pressure of 0.15 MPa, and the droplet velocity was higher under the pressure of 0.35 MPa in the near field. From the comparison between pressures, it was found that higher pressure produced a smaller droplet size due to the stronger impact force that caused the liquid film to break.

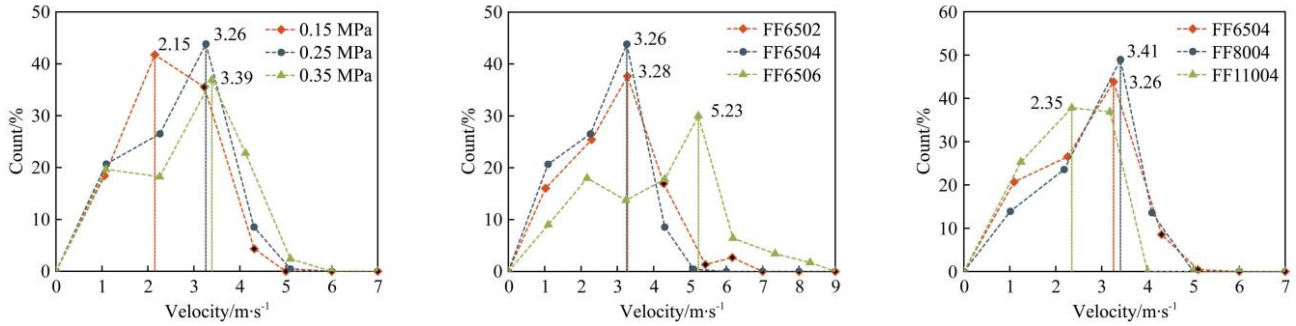

a. Relative number distribution of droplet velocity at 0.15 MPa, 0.25 MPa, 0.35 MPa (FF6504)

b. Relative number distribution of droplet velocity at FF6502, FF6504, FF6506

c. Relative number distribution of droplet velocity at FF6504, FF8004, FF11004

Figure 7 Relative number distribution of droplet velocity under different conditions

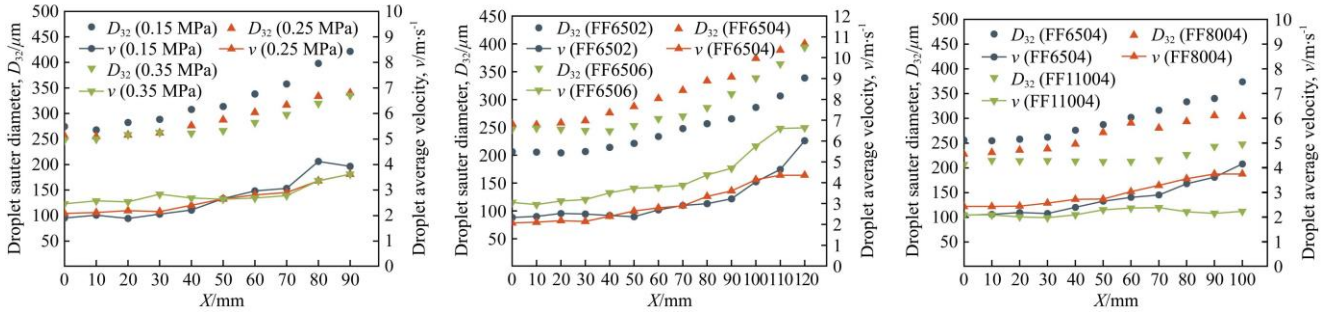

a. 0.15 MPa, 0.25 MPa, 0.35 MPa (FF6504)

b. FF6502, FF6504, FF6506

c. FF6504, FF8004, FF11004

Figure 8 Variations of droplet D_{32} and average velocity with axial distance under different conditions

Figure 8b depicts D_{32} and the average velocity along the radial distance under three different flow models (FF6502, FF6504, FF6506), the test pressure was 0.25 MPa. The difference is that D_{32} under different flow models was obvious, and the result of FF6504 nozzle was higher than the other two groups. All three groups gradually increased. The velocities of the three groups of nozzles were also increasing, but the differences between the types and the particle size comparison results were different. The velocity of FF6506 was higher than the other two groups. From the analysis of the changing trend, the upward trend of nozzles FF6502 and FF6506 was obvious, unlike the gentle change trend of FF6504, in contrast, there were more low-velocity droplets and the narrower velocity distribution interval in the latter atomization field. The droplet properties in the atomization field of the FF6504 nozzle at the pressure of 0.25 MPa were relatively stable, which also had advantageous uniformity.

Figure 8c shows the variation of SMD and average velocity along the radial distance from the spray center to the outside (left side) under three spray angles, namely, 65°, 80°, 110°. The test pressure was 0.25 MPa. Under the three sets of spray angles, the closer to the distal end, the greater the value of D_{32}. Among them, the particle size increase rate of FF6504 nozzle was more stable, and the particle size change trend of FF8004 nozzle showed more obvious fluctuations. Although FF11004 was increasing, there was little difference between D_{32} at the proximal and distal ends. In the velocity comparison, the average velocity of the FF8004 nozzle was higher than the other two groups, and the FF6504 had the largest velocity distribution range. The average velocity of FF11004 was relatively small, and there was no significant difference in velocity from the center to the edge of the spray.

3.3 Comparison of deposition model to spray experiment

The atomization field characteristics provided a more accurate delineation of the nozzle. On a microscopic level, all droplet sizes and velocities within the atomization field were determined which were used to calculate the deposition efficiency based on the impact discrimination. In order to establish a further high-correlation relationship between the atomization field characteristics and the deposition and explore the internal mechanism, the combined effects of the physical and chemical properties of the droplets and the deposition surface characteristics were considered in the model. The bounce and shatter threshold equations in the model were currently the mainstream methods for judging the behavior of the droplet interface. The model established in this study was based on the equation, and used the droplet size and velocity information of the atomization field as initial conditions to distinguish the droplet impact behavior. In the calculation process, the rebound droplets were removed, and the flow distribution figure of the remaining droplet size was obtained. In addition, the droplet diameter distribution figure included the number distribution and the volume or mass distribution. It should be clear that the application behavior was a mass transfer process. Therefore, this article used the mass or volume of the particle size distribution as the statistical quantity.

Contact angles for water and tartrazine mixture on strawberry and chrysanthemum are shown in Table 8. The critical impingement factors (K_{crit}) used for strawberry and chrysanthemum were 117 and 134 respectively.

Table 8 Contact angle of deionized water and sprayed liquid (°)

Plant	Water	Tartrazine solution	20% acetone	50% acetone
Strawberry	82.0	84.9	67.5	36.1
Chrysanthemum	82.3	83.0	39.8	16.0

Experimental impact outcomes for droplets on strawberry leaves are shown in Figure 9. In addition, the red and black function curves represent the strawberry and chrysanthemum shatter boundaries, respectively. If the droplet symbol appears on the upper side of the curve, it means that splashing will occur. Calculations found that the droplets rarely rebound or splash when hitting chrysanthemum leaves, so it is not marked in Figure 9. This situation could also be intuitively reflected in the splash threshold curve. Obviously, the splash threshold of chrysanthemum was higher.

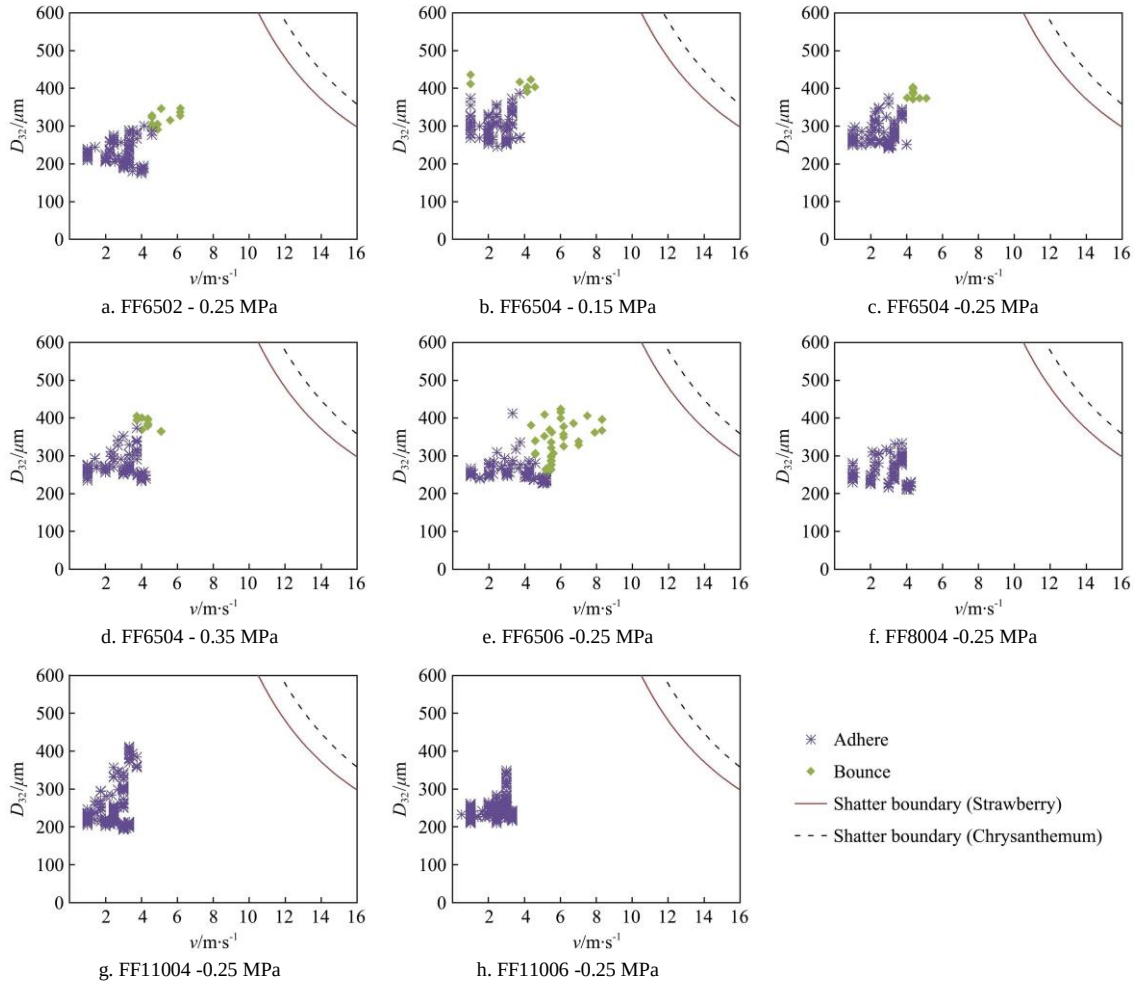

a. FF6502 - 0.25 MPa b. FF6504 - 0.15 MPa c. FF6504 -0.25 MPa

d. FF6504 - 0.35 MPa e. FF6506 -0.25 MPa f. FF8004 -0.25 MPa

g. FF11004 -0.25 MPa h. FF11006 -0.25 MPa

Figure 9 Discriminate the behavior of droplets hitting strawberry and chrysanthemum leaves under different conditions

In the prediction of strawberry impact behavior, only adhesion and rebound were found. The adhesion droplets were mostly located at the lower left position of the coordinate, which corresponded to a smaller diameter and velocity. The result of splashing was distributed above the curve in the upper right corner, corresponding to high velocity and large diameter. Among the droplet interface behaviors exhibited by comprehensive factors, the droplets sprayed from FF6506 bounced most, accounting for 30.3% of the total particle number. In addition, the proportion of bouncing droplets sprayed from FF6504 rose with increasing pressure and rose rapidly at 0.35 MPa. There was no rebound behavior in the calculation of the droplets sprayed from nozzles at 80 °and 110 °.

Figure 10 shows all the actual deposition experimental data. The experimental results will be analyzed below in conjunction with the transport model.

Figure 11a shows the flow distribution of droplet diameters under different pressures. The selected nozzle was FF6504. The solid line represents strawberry and the dotted line represents chrysanthemum. Figure 11b shows the deposit retention under the corresponding conditions. For ease of presentation, “S” and “C” in the legend mean strawberry and chrysanthemum, respectively. The peak droplet diameters of strawberry leaves under the pressure of 0.25 MPa and 0.35 MPa were the same, which were both located at 250-260 μm, but the latter accounted for a higher proportion, reaching 33.5%. The droplet diameter distribution curve under the pressure of 0.15MPa shifted to the right (the diameter becomes larger), and the peak point diameter accounted for 20.5%. Figure 11b showed that the leaf retention under 0.25 MPa was higher than the other two groups, which indicated that the droplets in the atomization field under 0.25 MPa were most likely to form effective deposits after removing the rebound and splashed droplets. The droplets rarely rebounded and splashed in the chrysanthemum leaf impact model, so the standard of *RS* could be used. The droplet diameters at the peak point at pressures of 0.15 MPa, 0.25 MPa, and 0.35 MPa were in the range of 260-270 μm, 250-260 μm, and 250-260 μm, respectively. The *RS* were 0.45, 0.43, 0.46, respectively. Figure 11b showed that the retention effect was the best under the condition of 0.25 MPa. In addition, under the same atomization field, the sediment retention of chrysanthemum was higher than that of strawberry. There were droplets larger than 400 μm in the chrysanthemum droplet diameter distribution, which would rebound and then be lost in the strawberry impact model.

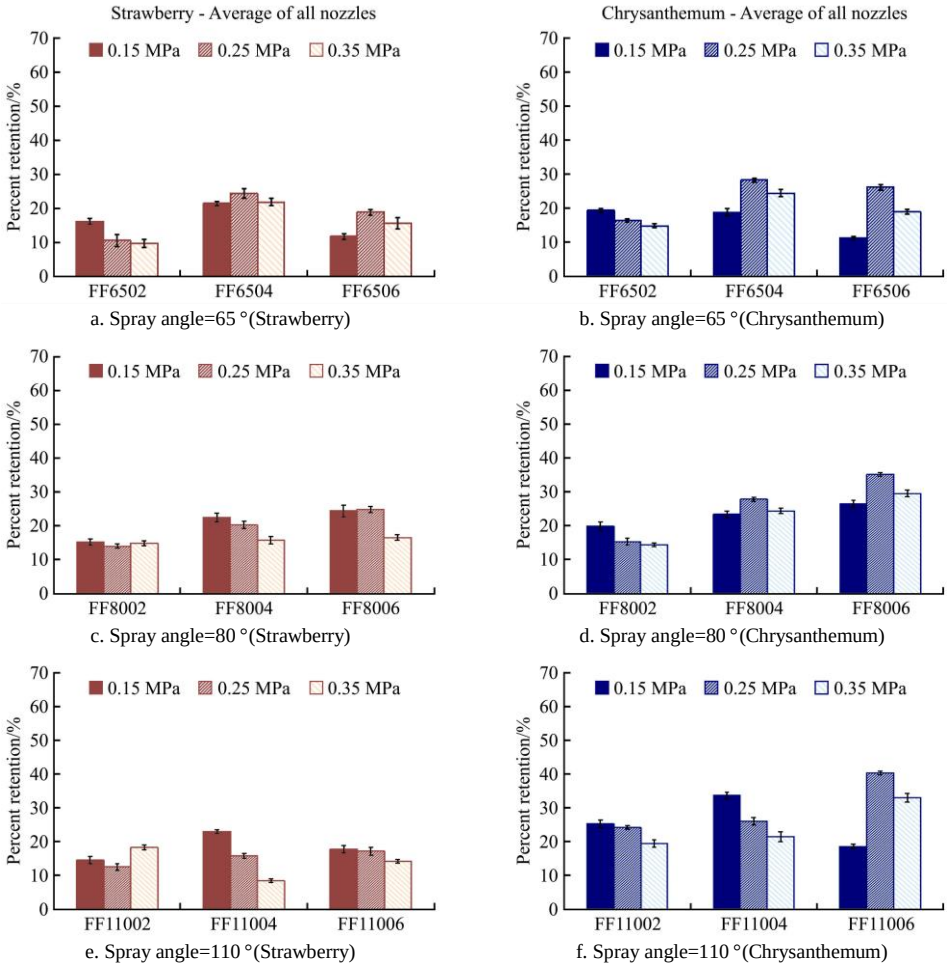

a. Spray angle=65 °(Strawberry) b. Spray angle=65 °(Chrysanthemum)

c. Spray angle=80 °(Strawberry) d. Spray angle=80 °(Chrysanthemum)

e. Spray angle=110 °(Strawberry) f. Spray angle=110 °(Chrysanthemum)

Figure 10 Percent retention of strawberry leaves and chrysanthemum leaves

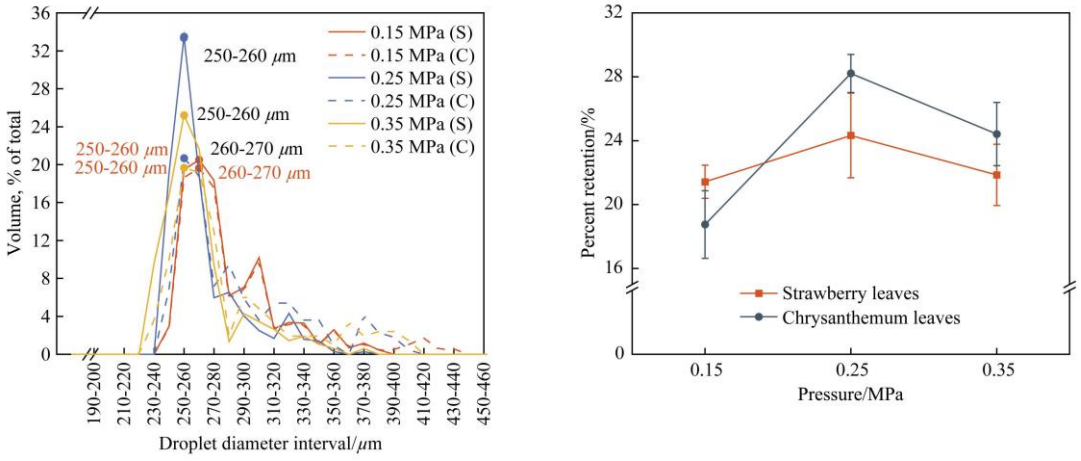

a. Droplet diameter flow distribution under three pressures b. The percent retention under three pressures

Figure 11 Droplet diameter flow distribution under three pressures and the percent retention under corresponding conditions (FF6504)

Figure 12a shows the flow distribution diagram of the droplet diameter under the three flow rate types, the selected pressure was 0.25 MPa. Figure 12b shows the plant retention under the corresponding conditions. In the strawberry impact model, the droplet diameter at the peak point of the FF6502 nozzle was the smallest at 200-210 μm, accounting for 21.4%, which was also the smallest. The distribution curve had a fluctuation in the range of 180-200 μm. Figure 12b showed that the deposition retention of the FF6502 nozzle was the lowest; The FF6504 nozzle had the largest droplet diameter at the peak point, in the range of 250- 260 μm, accounting for 33.5%, and the deposition efficiency was also the highest; The droplet distribution curve of the FF6506 nozzle began to move to the left, the peak droplet diameter was 240-250 μm, accounting for 32.3%, and the deposition rate was higher than that of the FF6502 nozzle. The peak point of the droplet diameter in the chrysanthemum impact model was overall smaller than that of the strawberry, and the concentration of the distribution curve was relatively inferior. The peak droplet diameters of nozzles FF6502, FF6504, and FF6506 were in the ranges of 200-210 μm, 250-260 μm, 240-250 μm, respectively. Compared with FF6504, the FF6506 distribution curve shifted to the left, but the trend was similar. The droplet diameter distribution of the FF6502 nozzle was poorly concentrated, and the effective deposition was low. The

deposition effect of FF6504 nozzle was the best. In addition, the selection of the flow rate model is needed to match the pressure. Too low pressure would result in a poorly concentrated droplet size distribution, and too high would result in too large initial distribution, all of which had varying degrees of impact on efficiency.

Figure 13a presents the flow distribution diagram of the droplet diameter under different spray angles. Figure 13b shows the deposition under the corresponding conditions. The difference in droplet diameter distribution was obvious at different angles. The concentrated distribution area moved to the left as the angle increased, and the peak droplet diameters were 250-260 μm, 220-230 μm, 200-210 μm, respectively. The droplet distribution trend of FF8004 nozzle was similar to nozzle FF6504, but its deposition efficiency was only 20.2%, which was lower than 24.3% of nozzle FF6504. The peak droplet diameter of the nozzle FF11004 was smaller in the range of 200-210 μm, accounting for 27.1%, and its deposition efficiency was only 15.9%. It is reasonable to speculate that 250-260 μm was the dominant droplet diameter in the strawberry impact model. In the chrysanthemum impact model, the peak point droplet diameters of nozzles FF6504, FF8004, and FF11004 were 250-260 μm, 220-230 μm, 210-220 μm, and *RS* were 0.43, 0.32, and 0.66, respectively. The overall deposition efficiency showed a decreasing trend with a small difference in the deposition detection experiment.

The results showed that the impact model situation of strawberry leaves was more satisfactory, and the results of chrysanthemum leaves had some errors, which could be analyzed from the initial morphology of the sprayed test plants. In the spraying experiment, strawberry leaves were spread out in the test plane without mutual shading between leaves, which could be regarded as the impact situation where the leaves remained horizontal. In contrast, chrysanthemum leaves were at an angle to the horizontal plane and had some shoots wrapped in the middle, which affected the determination of deposition per unit leaf area. Dorr[35] and Zabkiewicz[49] have likewise performed measurements of spray retention in the whole plants, and this deposition model cannot be applied to complex morphological plants, i.e., when leaf overlap or excessive initial leaf inclination occurs. This will be an issue that we need to explore further in the future.

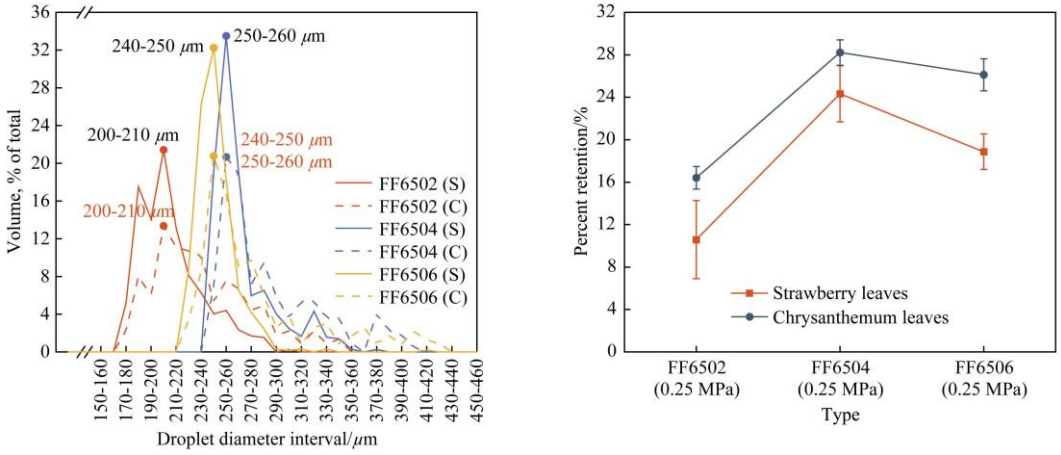

a. Droplet diameter flow distribution under three flow rate types b. The percent retention under three flow rate types

Figure 12 Droplet diameter flow distribution under three flow rate types and the percent retention under corresponding conditions

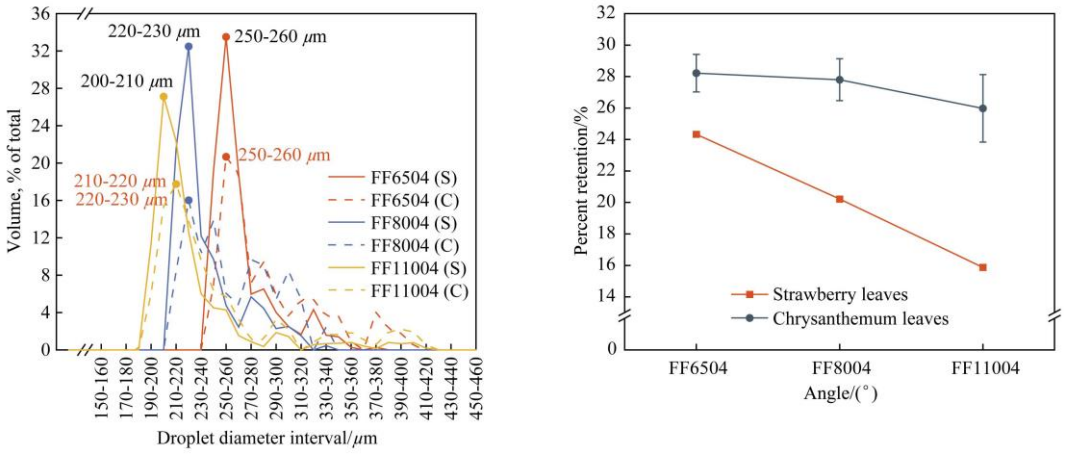

a. Droplet diameter flow distribution under three spray angles b. The percent retention under three spray angles

Figure 13 Droplet diameter flow distribution under three spray angles and the percent retention under corresponding conditions

4 Conclusions

In this study, PDPA technology was used to describe the characteristics of the atomization field of flat fan nozzles under different conditions, and a droplet impact model was established to explore the relationship between the characteristics of the atomization field and the deposition efficiency. Experimental conditions include three sets of pressure, at 0.15 MPa, 0.25 MPa, 0.35 MPa; three sets of flow models, at 02, 04, 06; and three sets of spray angles, at 65°, 80°, 110°. Mainly conclusions include as follows:

1) The cumulative distribution of droplet diameter could be perfectly fitted by the Rosin-Rammler correlation. The uniformity constant, characteristic droplet size, and relative size

range of the atomization field of the flat fan nozzle under different conditions were presented, which provided important initial input parameters for spray simulation.

2) The droplet SMD of the atomization field showed a downward trend with the increase of spray pressure; The droplet SMD of the atomization field increased first and then decreased with the increase of nozzle flow rate type; The droplet SMD first decreased and then rose with the increase of the spray angle. The above peak velocity showed the opposite trend to the corresponding SMD. In addition, it was found that the droplet SMD and average velocity gradually decreased with increasing radial distance. As the spray angle increased, the difference in droplet properties between the near-field area and the far-field area in the atomization field became smaller.

3) The impact model determined the behavior of the droplets in the actual spray area based on the initial distribution of the droplets, which narrowed the interval for the selection of the optimal droplet diameter. High-velocity droplets were eliminated in the model calculation, which reduced the influence of velocity factors on deposition and promoted the size range as the standard for nozzle selection. The results of this study showed that the optimal droplet diameter ranges of strawberry leaves and chrysanthemum leaves were 250-270 μm and 240-260 μm, respectively. In addition, the smaller *RS* would lead to better deposition effect.

4) The initial distribution of droplets in the spray nozzle atomization field directly affected the deposition behavior, but it was found that the deposition law was affected by the combination of the characteristics of the atomization field instead of inference by a single variable. This paper proposed that the unit spatial density of droplet could be used as a link to establish the correlation between the characteristics of the atomization field and the deposition efficiency. The results showed that the method clarified the law between characteristic variables and deposition efficiency. Future research can take more complex models such as the interaction between droplets into the atomization field to realize the prediction of pesticide deposition based on this method.

Acknowledgements

This research was supported by the Ningxia Key Research and Development Program (Grant No. 2019BBF02009).

Nomenclature

Symbol	Description
FF	Flat fan
PDPA	Phase doppler particle analyzer
PMS	Particle measuring system
PPP	Plant protection products
RS	Relative span
SMD	Sauter Mean Diameter
A	Deposition percentage, %
$CA_{20\%acetone}$, $CA_{50\%acetone}$	Contact angles made by a droplet of either 20% acetone or 50% acetone
D	Droplet diameter, mm
D_0	Characteristic particle size, mm
D_{10}	Arithmetic mean diameter, mm
D_{20}	Surface mean diameter, mm
D_{30}	Volume mean diameter, mm
D_{32}	Sauter mean diameter or the diameter of a drop having the same volume to surface area ratio as the total volume of all the drops to the total surface area of all the drops, mm
D_{v10}, D_{v50}, D_{v90}	Volume diameter below which smaller droplets constitute 10%, 50% and 90% of the total volume, respectively
E_{ERE}	Excess rebound energy
K	Composite parameters, comprehensive characteristics of droplets before impact
K_{crit}	Characteristics of the impact surface
m_l	Leaf surface deposition mass, g
m_a	Target collection mass, g
N	Number of droplets
Oh	Ohnesorge number
Re	Reynolds number
S_l	Leaf area, cm^2
S_a	Artificial target area, cm^2
v	Droplet impact velocity, m/s
v_n	Velocity component in the vertical direction
V	Volume of the droplet, m^3
V_{100}, V_{200}	Proportion of total volume of droplets smaller than 100 mm, 200 mm in diameters, respectively, %
We	Weber number
y	Cumulative fraction, %
ρ	Density, $kg \cdot m^{-3}$
μ	Fluid viscosity, kg/(m s)
σ	Surface tension of spray droplet, kg/s^2
α	Impingement angle, (°)
θ_e	Static contact angle, (°)
δ	Uniformity constant

[References]

[1] Appah S, Wang P, Ou M X, Gong C, Jia W D. Review of electrostatic system parameters, charged droplets characteristics and substrate impact behavior from pesticides spraying. Int J Agric & Biol Eng, 2019; 12(2): 1–9.

[2] Ru Y, Liu Y Y, Qu R J, Patel M K. Experimental study on spraying performance of biological pesticides in aerial rotary cage nozzle. Int J Agric & Biol Eng, 2020; 13(6): 1–6.

[3] Wang L H, Lan Y B, Yue X J, Ling K J, Cen Z Z, Cheng Z Y, et al. Vision-based adaptive variable rate spraying approach for unmanned aerial vehicles. Int J Agric & Biol Eng, 2019; 12(3): 18–26.

[4] Asaei H, Jafari A, Loghavi M. Site-specific orchard sprayer equipped with machine vision for chemical usage management. Computers and Electronics in Agriculture, 2019; 162: 431–439.

[5] Yazbeck T, Bohrer G, De Roo F, Mauder M, Bakshi B. Effects of spatial heterogeneity of leaf density and crown spacing of canopy patches on dry deposition rates. Agricultural and Forest Meteorology, 2021; 306: 108440. doi: 10.1016/j.agrformet.2021.108440.

[6] Torrent X, Garcerá C, Moltó E, Chueca P, Abad R, Grafulla C, et al. Comparison between standard and drift reducing nozzles for pesticide application in citrus: Part I. Effects on wind tunnel and field spray drift. Crop Protection, 2017; 96: 130–143.

[7] Chen S D, Lan Y B, Zhou Z Y, Deng X L, Wang J. Research advances of the drift reducing technologies in application of agricultural aviation spraying. Int J Agric & Biol Eng, 2021; 14(5): 1–10.

[8] Jeyaratnam J. Acute pesticide poisoning: A major global health problem. World Health Stat Q, 1990; 43(3): 139–144.

[9] Wagner M, Lin K, Oh W D, Lisak G. Metal-organic frameworks for pesticidal persistent organic pollutants detection and adsorption - A mini review. Journal of Hazardous Materials, 2021; 413: 125325. doi: 10.1016/j.jhazmat.2021.125325.

[10] Josserand C, Thoroddsen S T. Drop impact on a solid surface. Annual Review of Fluid Mechanics, 2016; 48(1): 365–391.

[11] Ma X H, Lan Z, Wang K, Chen Y S, Cheng Y Q, Du B G, et al. Dancing droplet: Interface phenomena and process regulation. CIESC Journal, 2018; 69(1): 9–43. (in Chinese)

[12] Delele M A, Nuyttens D, Duga A T, Ambaw A, Lebeau F, Nicolai B M, et al. Predicting the dynamic impact behaviour of spray droplets on flat plant surfaces. Soft Matter, 2016; 12(34): 7195–7211.

[13] Li H, Niu X X, Ding L, Tahir A S, Guo C L, Chai J J, et al. Dynamic spreading characteristics of droplet impinging soybean leaves. Int J Agric & Biol Eng, 2021; 14(3): 32–45.

[14] Song M R, Hu D, Zheng X F, Wang L X, Jiang L. Enhancing droplet deposition on wired and curved superhydrophobic leaves. ACS Nano,

2019; 13(7): 7966–7974.
[15] Zhu L, Ge J, Qi Y, Chen Q, Hua, R M, Luo F, et al. Droplet impingement behavior analysis on the leaf surface of Shu-ChaZao under different pesticide formulations. Comput Electron Agric, 2018; 144: 16–25.
[16] Dorr G J, Wang S, Mayo L C, Mccue S W, Forster W A, Hanan J, et al. Impaction of spray droplets on leaves: Influence of formulation and leaf character on shatter, bounce and adhesion. Experiments in Fluids, 2015; 56(7): 1–17.
[17] Forster W A, Mercer G N, Schou W C. Process-driven models for spray droplet shatter, adhesion or bounce. Proceedings of the 9th International Symposium on Adjuvants for Agrochemicals. Freising, Germany: Technical University of Munich, 2010; 16: 277–285.
[18] Mao T, Kuhn D C S, Tran H. Spread and rebound of liquid droplets upon impact on flat surfaces. Aiche Journal, 1997; 43(9): 2169–2179.
[19] Mundo C, Sommerfeld M, Tropea C. Droplet-wall collisions - Experimental studies of the deformation and break-up process. Int J Multiphas Flow, 1995; 21(2): 151–173.
[20] Lee S, Park S. Spray atomization characteristics of a GDI injector equipped with a group-hole nozzle. Fuel, 2014; 137: 50–59.
[21] Nuyttens D, Baetens K, Schampheleire M D, Sonck B. Effect of nozzle type, size and pressure on spray droplet characteristics. Biosystems Engineering, 2007; 97(3): 333–345.
[22] Zhou Z F, Yin J, Yang X Y, Chen B, Liu B. Experimental investigation on the macroscopic spray and microscopic droplet diameter, velocity and temperature of R404A flashing spray. Int J Heat Mass Transf, 2021; 177: 121546. doi: 10.1016/j.ijheatmasstransfer.2021.121546.
[23] Xue S D, Xi X, Lan Z, Wen R F, Ma X H. Longitudinal drift behaviors and spatial transport efficiency for spraying pesticide droplets. Int J Heat Mass Transf, 2021; 177: 121516. doi: 10.1016/j.ijheatmasstransfer.2021.121516.
[24] ASABE standard S572.1: Spray nozzle classification by droplet spectra. ASABE, St. Joseph, 2009.
[25] Tuck C R, Ellis M B, Miller P. Techniques for measurement of droplet size and velocity distributions in agricultural sprays. Crop protection, 1997; 16(7): 619–628.
[26] Derksen R C, Ozkan H E, Fox R D, Brazee R D. Droplet spectra and wind tunnel evaluation of venturi and pre-orifice nozzles. Transactions of the ASAE, 1999; 42(6): 1573–1580.
[27] Teske M E, Thistle H W, Hewitt A J, Kirk I W. Conversion of droplet size distributions from PMS optical array probe to Malvern laser diffraction. Atomization and Sprays, 2002; 12(1-3): 267–281.
[28] Kashdan J T, Shrimpton J S, Whybrew A. A digital image analysis technique for quantitative characterisation of high-speed sprays. Optics and Lasers in Engineering, 2007; 45(1): 106–115.
[29] Torrent X, Gregorio E, Douzals J P, Tinet C, Planas S. Assessment of spray drift potential reduction for hollow-cone nozzles: Part 1. Classification using indirect methods. Science of the Total Environment, 2019; 692: 1322–1333.
[30] Zhang H C, Zhou H P, Zheng J Q, Liao J, Hewitt A J. Adjuvant's influence to droplet size based on forestry pests' prevention with ground and air chemical application. Scientia Silvae Sinicae, 2020; 56(5): 118–129. (in Chinese)
[31] Bing X H, Sun D Z, Song S R, Xue X Y, Dai Q F. Simulation and experimental research on droplet flow characteristics and deposition in airflow field. Int J Agric & Biol Eng, 2020; 13(6): 16–24.
[32] Couvidat F, Bedos C, Gagnaire N, Carra M, Ruelle B, Martin P, et al. Simulating the impact of volatilization on atmospheric concentrations of pesticides with the 3D chemistry-transport model CHIMERE: Method development and application to S-metolachlor and folpet. Journal of Hazardous Materials, 2021; 424(Part B): 127497. doi: 10.1016/j.jhazmat.2021.127497.
[33] Lu X Y, Gong Y, Liu D J, Wang G, Chen X, Zhang X, et al. CFD simulation and experiment on the flow field of air-assisted ultra-low-volume sprayers in facilities. Int J Agric & Biol Eng, 2021; 14(2): 26–34.
[34] Cao Y L, Yu F H, Xu T Y, Du W, Guo Z H, Zhang H Y. Effects of plant protection UAV-based spraying on the vertical distribution of droplet deposition on Japonica rice plants in Northeast China. Int J Agric & Biol Eng, 2021; 14(5): 27–34.
[35] Dorr G J, Forster W A, Mayo L C, McCue S W, Kempthorne D M, Hanan J, et al. Spray retention on whole plants: modelling, simulations and experiments. Crop Protection, 2016; 88: 118–130.
[36] Matsukawa-Nakata M, Nguyen H T, Bui T T B, Van Le H, Nguyen C H, Kobori Y. Spatial evaluation of the pesticide application method by farmers in a paddy field in the northern part of Vietnam. Applied Entomology and Zoology, 2019; 54(4): 451–457.
[37] Gregorio E, Torrent X, Planas S, Rosell-Polo J R. Assessment of spray drift potential reduction for hollow-cone nozzles: Part 2. LiDAR technique. Science of The Total Environment, 2019; 687: 967–977.
[38] Grella M, Marucco P, Balsari P. Toward a new method to classify the airblast sprayers according to their potential drift reduction: comparison of direct and new indirect measurement methods. Pest Management Science, 2019; 75(8): 2219–2235.
[39] Nuyttens D, Zwertvaegher I K, Dekeyser D. Spray drift assessment of different application techniques using a drift test bench and comparison with other assessment methods. Biosystems Engineering, 2017; 154: 14–24.
[40] Sinha R, Ranjan R, Khot L R, Hoheisel G A, Grieshop M J. Drift potential from a solid set canopy delivery system and an axial-fan air-assisted sprayer during applications in grapevines. Biosystems Engineering, 2019; 188: 207–216.
[41] Wang C L, Zeng A J, He X K, Song J L, Gao W L. Spray drift characteristics test of unmanned aerial vehicle spray unit under wind tunnel conditions. Int J Agric & Biol Eng, 2020; 13(3): 13–21.
[42] Garcerá C, Román C, Moltó E, Abad R, Insa J A, Torrent X, et al. Comparison between standard and drift reducing nozzles for pesticide application in citrus: Part II. Effects on canopy spray distribution, control efficacy of Aonidiella aurantii (Maskell), beneficial parasitoids and pesticide residues on fruit. Crop Protection, 2017; 94: 83–96.
[43] Gentil-Sergent C, Basset-Mens C, Gaab J, Mottes C, Melero C, Fantke P. Quantifying pesticide emission fractions for tropical conditions. Chemosphere, 2021; 275: 130014. doi: 10.1016/j.chemosphere.2021.130014.
[44] Gu C C, Liu Z J, Pan G T, Pu Y J, Yang F Z. Optimization of working parameters for 3MGY-200 axial air-assisted sprayer in kiwifruit orchards. Int J Agric & Biol Eng, 2020; 13(2): 81–91.
[45] Bolat A, Özlüoymak Ö B. Evaluation of performances of different types of spray nozzles in site-specific pesticide spraying. Semina: Ciências Agrárias, 2020; 41(4): 1199–1212.
[46] Deren K, Szewczyk A, Sekutowski T R. Effect of the type of preparation and spraying parameters on zinc deposition on soybean plants. Int J Environ Sci Tech, 2019; 16(7): 3447–3454.
[47] Massinon M, Cock N D, Salah S, Lebeau F. Reduced span spray-Part 1: Retention. in Alexander L, Cooper S, Cross J, et al. (Eds) International Advances in Pesticide Application, Association of Applied Biologists, Wellesbourne, United Kingdom, 2016.
[48] Wang Z W, Di S S, Qi P P, Xu H, Zhao H Y, Wang X Q. Dissipation, accumulation and risk assessment of fungicides after repeated spraying on greenhouse strawberry. Science of The Total Environment, 2021; 758: 144067. doi: 10.1016/j.scitotenv.2020.144067.
[49] Zabkiewicz J A, Pethiyagoda R, Forster W A, van Leeuwen R, Moroney T J, McCue S W. Simulating spray droplet impaction outcomes: Comparison with experimental data. Pest Management Science, 2020; 76(10): 3469–3476.